designs

MDPI

Article

Battery Housing for Electric Vehicles, a Durability Assessment Review

Moises Jimenez-Martinez [1,*,†], José Luis Valencia-Sánchez [1,†], Sergio G. Torres-Cedillo [2] and Jacinto Cortés-Pérez [2]

[1] Tecnologico de Monterrey, School of Engineering and Sciences, Via Atlixcayotl 5718, Puebla 72453, Mexico; a01325370@tec.mx
[2] Centro Tecnológico FES Aragón, Universidad Nacional Autónoma de México, Nezahualcóyotl 57171, Mexico; sergiotorres98@aragon.unam.mx (S.G.T.-C.); jacop@unam.mx (J.C.-P.)
* Correspondence: moisesjimenezmartinez@gmail.com
† These authors contributed equally to this work.

Abstract: Recent research emphasizes the growing use of advanced composite materials in modern transportation, highlighting their superior weight-to-strength ratio. These materials are increasingly replacing steel and aluminium in housings to enhance sustainability, improve efficiency, and reduce emissions. Considering these advancements, this article reviews recent studies on composite materials, focusing on fatigue life assessment models. These models, which include performance degradation, progressive damage, and S–N curve models, are essential for ensuring the reliability of composite materials. It is noted that the fatigue damage process in composite materials is complex, as failure can occur in the matrix, reinforcement, or transitions such as interlaminar and intralaminar delamination. Additionally, the article critically examines the integration of artificial intelligence techniques for predicting the fatigue life of composite materials, offering a comprehensive analysis of methods used to indicate the mechanical properties of battery shell composites. Incorporating neural networks into fatigue life analysis significantly enhances prediction reliability. However, the model's accuracy depends heavily on the comprehensive data it includes, including material properties, loading conditions, and manufacturing processes, which help to reduce variability and ensure the precision of the predictions. This research underscores the importance of continued advancements and their significant scientific contributions to transportation sustainability, especially in the context of emerging artificial intelligence technologies.

Keywords: battery housing; artificial intelligence; composites materials; fatigue

check for updates

Citation: Jimenez-Martinez, M.; Valencia-Sánchez, J.L.; Torres-Cedillo, S.G.; Cortés-Pérez, J. Battery Housing for Electric Vehicles, a Durability Assessment Review. *Designs* **2024**, *8*, 113. https://doi.org/10.3390/designs8060113

Academic Editor: Junnian Wang

Received: 22 August 2024
Revised: 20 October 2024
Accepted: 29 October 2024
Published: 31 October 2024

Copyright: © 2024 by the authors. Licensee MDPI, Basel, Switzerland. This article is an open access article distributed under the terms and conditions of the Creative Commons Attribution (CC BY) license (https://creativecommons.org/licenses/by/4.0/).

1. Introduction

Mobility has been used to improve societal development due to the feasibility of moving across medium and long distances. However, at the same time, the majority of propulsion systems are fuelled by fossil energy sources, generating a worldwide impact from the pollution generated by internal combustion engines. Approximately 30% of the pollution generated by vehicle emissions occurs in the United States [1]. Moreover, nearly 25% of greenhouse emissions occur in Europe [2]. To reduce these emissions, alternative powertrain systems have been proposed to reduce the emissions from tank to wheel to zero. Regulations are defined for new vehicles regarding CO_2 emissions. The Environmental Protection Agency (*EPA*) defines 82.5 g/km for passenger vehicles manufactured before 2026, while in the European Union the limit is 95 g/km until 2025; this limit is expected to decrease by 30% in 2030 and become zero in 2035 [3,4].

To improve vehicle performance, an electric motor can be added to a vehicle, or the internal combustion engine (*ICE*) can be substituted by an electric motor. These vehicles can be classified based on the hybridization level: microhybrid or start/stop, mild hybrid, full hybrid, plug-in hybrid, and electric [5–8].

Hybrid electric vehicles (*HEVs*) do not reduce hydrocarbon emissions and can even increase carbon monoxide emissions. This occurs because frequent engine stops and restarts prevent the complete combustion of carbon fuels. Consequently, the catalyst cannot maintain a constant temperature, impairing its ability to function correctly and release combustion gases efficiently. To address these issues, fully electric vehicles are considered the best option for minimizing emissions from tank to wheel. Although electric vehicles themselves do not emit pollutants, the electricity generation process can result in significant emissions. Thus, the environmental benefits of electric cars may be limited unless cleaner energy sources are adopted [9].

The powertrain must overcome inertia loads, such as losses from the engine to the wheel. The energy supplied by the *ICE* is transmitted to the wheels; this transmission process from the engine through the powertrain components has its own losses and depends on its efficiency as well as vehicle requirements and power demand. It depends not only on the internal efficiency of the powertrain components but also on the road conditions (slope, type of road) and the temporal characteristics of the vehicle, such as the passenger number, cargo, rolling resistance, fuel characteristics, drag coefficient, and residual brake [10]. To reduce these losses, powertrain configurations have improved based on vehicle packing. Figure 1 shows different architectures for HEVs: series (Figure 1a), parallel (Figure 1b), hybrid (Figure 1c), and all-wheel drive (Figure 1d) architectures.

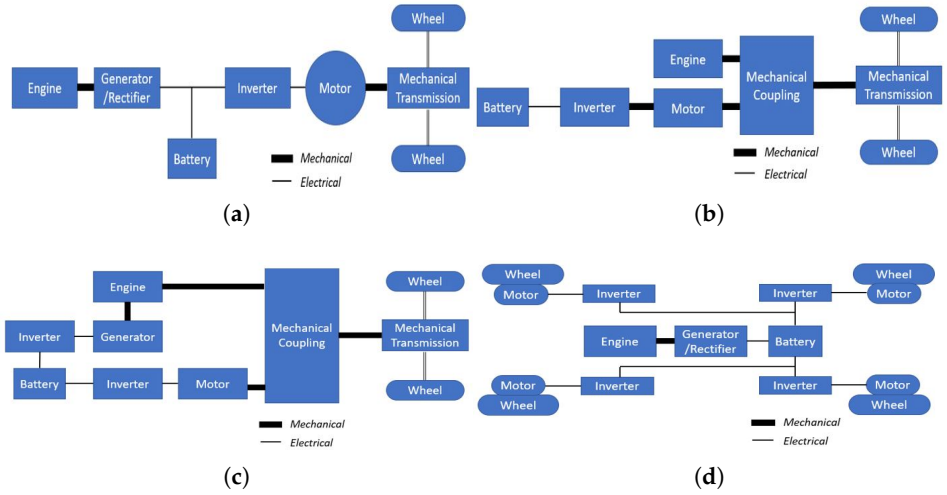


Figure 1. Packing of HEVs: (**a**) series, (**b**) parallel, (**c**) series–parallel, and (**d**) all-wheel drive (AWD).

Batteries generate energy through a chemical process and are used in devices ranging from cell phones and e-bikes to cargo vehicles. However, one of the biggest challenges in transitioning from fossil fuel vehicles to battery-powered ones is the additional weight. This issue is particularly significant for unmanned aerial vehicles, where the battery can account for 20–40% of the total weight [11,12]. However, electric vehicles can reduce emissions by 84% compared with internal combustion engine emissions [1]. The use of lightweight materials increases vehicle autonomy through weight reduction [13], and the battery pack is an essential component of the battery system and contributes to improving vehicle performance and autonomy. Initially, vehicle performance was enhanced by a chemical approach that modified the energy density used in the chemical reactions. Some rechargeable technologies for batteries include magnesium ions, hydrogen, and the most commonly used lithium ions [10,14–16]. The other way to improve vehicle performance is to reduce the weight of the battery pack while fixing the chemical process [17,18].

Temperature is an important factor in battery operation due to its effect on efficiency and correct operation; by nature, heat is generated during the chemical process to obtain energy, and it has an optimal range of 15–50 °C and a difference below 5 °C between cells. To reach these limits, thermal management systems (BTMSs) are particularly important and include liquid cooling, air cooling, and phase change materials (PCMs). During the

charging and discharging of batteries, a chemical process is generated that generates heat. Keeping the system within an optimal temperature range prevents battery discharge and aging, as well as avoiding operating risks due to overheating. For this purpose, the thermal management system is used to control and dissipate heat through convection, radiation, and conduction. Duct arrangements can be used to work by exchanging heat, using materials such as PCMs [19–22]. PCMs contribute to heat dissipation and battery cooling. During the transient phase change process, a cooling effect is generated through the PCMs absorbing and dissipating heat [23–29].

The use of lightweight materials is an essential part of the mobility industry to reduce the impact of the carbon footprint during vehicle operation. While there are areas of opportunity in certain regions for clean energy generation, tank-to-wheel emissions are reduced or eliminated. An essential element for the migration and implementation of hybrid and electric vehicles is the battery, which uses a housing that protects it from impacts, electromagnetic fields, water absorption, and mechanical loads. The reduction of the housing weight contributes to the autonomy of the vehicle. Although the response has been analyzed in vibrations, low impact, and thermal loads, no work has been done to review the fatigue life in composite materials. This work reviews the main load cases, the materials, and analysis methods that allow the evaluation of the durability of the battery housings. Section 2 reviews aspects related to the battery housing, describes its functions, and summarizes the main materials used for its manufacture. Section 3 describes the process of analysis of fatigue in composite materials, for which the main characteristics of load signals, counting processes, as well as damage models for predicting and determining fatigue useful life are described. Section 4 focuses on the use of artificial intelligence for fatigue life prediction. The architecture and definition of characteristics of the neural network to predict durability depend on the characteristics of the damage process; to understand it, the structure of the networks as well as the different types of neural networks are described. *NARX* dynamic networks are included, which can be used to predict the response as a function of time as in the case of variable amplitude load histories.

2. Battery Housing

Battery packs contribute to the operational functions of a battery not only through packaging but also through battery management, connection, cooling, pressure relief, electromagnetic shielding [12,30], and the ability to account for leakage and corrosion protection. Additionally, load vibrations can affect electrical continuity or mechanical degradation, leading to fatigue failure [31–33]. Crushing and crash loads can generate intrusions on a battery pack, generating thermal runaway because the battery cells are connected in series or parallel to the thermal runaway and can reach temperatures of 1500 °C [34]. Additionally, fire shielding postpones fire and toxic gas propagation with a risk of explosion [35–38]. Housing also works through electromagnetic shielding [36,39], after which the components can be recycled [40,41].

The battery housing must simultaneously meet the structural and operational requirements and be as light as possible with the ability to reach an approximately 30% weight reduction [42], considering that the battery system can reach 400 kg for a 50 kW/h system with a battery case of approximately 80 kg. This weight impacts vehicle performance, and it also has a cost of 35–50% of the vehicle structure [43]. Based on their mechanical properties, common materials for housings include steel (*Hitachi metals*, *Edag*), aluminium (*Novalis − Co*), and composite materials (*SGL Carbon* [44], *Kautex Textron GmbH & Co. KG*. [45], *Syensqo* [46] *Plastics today* [47], *IDTechEx* [48], *BCP* [49], *Hunstman* [50]), or a hybrid approach, as proposed by *Rhling Automotive Co*. [51].

The composite material combined with the manufacturing process reduces the weight and, at the same time, reduces the number of components, which decreases the assembly complexity. While metal-based housing has shielding properties due to its conductivity, conductive coatings or magnetic fillers can be added to composites [52]. Due to its feasibility,

extrusion and injection moulding can be used to melt the polymer, solidify it during cooling, and improve its mechanical performance with short or long fibers [53,54].

3. Fatigue in Composites

Fiber-reinforced composites are the result of the combination of materials applied in different industries, such as the aerospace, automotive, and marine industries. They have the advantages of combining the advantages of each material, as well as improving the mechanical properties of impact, buckling, fatigue, and vibration [55]. The reinforcement can be random (chopped) or through short or long fibers (Figure 2). Depending on the reinforcement definition, which affects the mechanical properties, fiber alignment can increase the tensile strength [56].

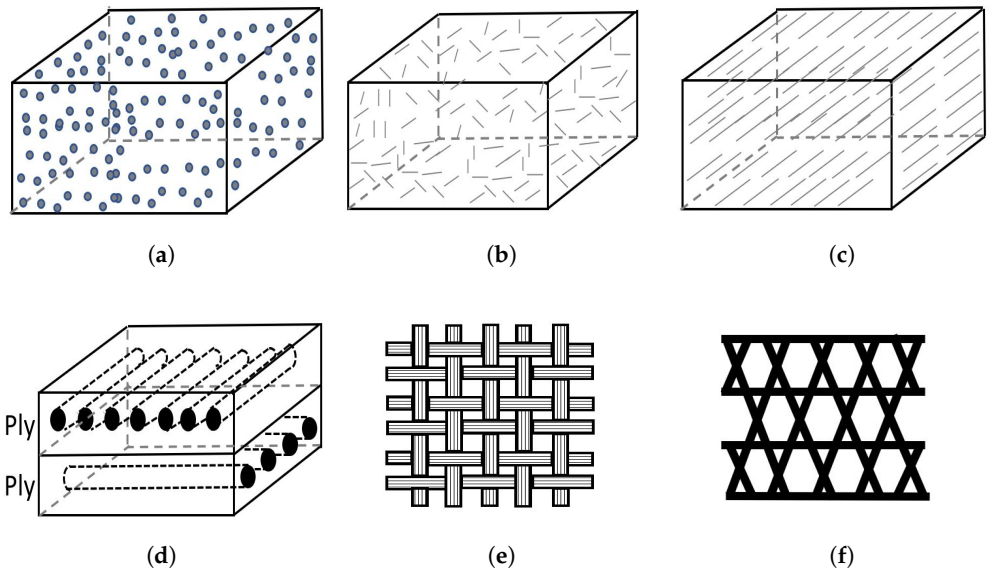


Figure 2. Manufacturing processes for composites: (**a**) particulate composite (quasi-isotropic), (**b**) short fiber composite, (**c**) long fiber composite, (**d**) laminate, (**e**) woven fabric (biaxial weave), and (**f**) woven fabric (triaxial weave).

Fatigue failure is an accumulated process developed by a cyclic load, and most failures are caused by damage to the component on the matrix, on the reinforcement or in its cohesive area, resulting in a process known as delamination [57–59]. In composite materials, fatigue life assessment models can be categorized into property degradation models, progressive damage models, and S–N curve models [60]. Failure is the component response change resulting from fiber fracture, matrix cracking, delamination, or a combination of failure mechanisms [61,62]. Fatigue assessment is complex because it must consider not only the loads, design, materials, and manufacturing processes, but also the changes in all of these processes that modify the linked parameters (materials, loads, design, and manufacturing process) must be considered, as shown in Figure 3. The manufacturing process generates a series of changes that may eventually have an effect on the mechanical performance of various components. The same component design is based on a tolerance according to its operating characteristics and the interaction with other components. Even with the same supplier, materials have small variations in their properties. These variations are included as sources of variability. The source that has the greatest amount of dispersion is the load because the same component with different users generates a different response. In the case of vehicles, aggressive and conservative driving profiles exist. There are maneuvers or road conditions that could generate unexpected loads within the operation of the same vehicle or are defined as abuse when loading the vehicle to the limit, e.g., driving into a pothole. Crossing an irregular road at high speed or encountering a roadblock could also

affect the load. This not only generates an additional load but also a possible permanent deformation that modifies the properties of the component.

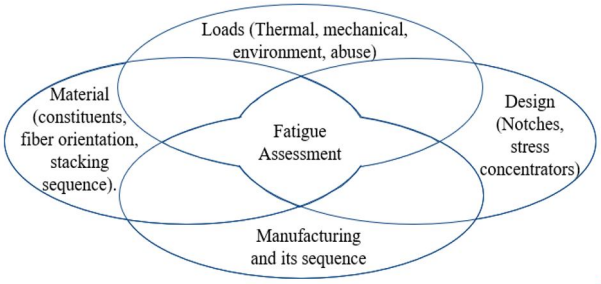


Figure 3. Factors in fatigue assessment.

Material performance depends not only on the constituent materials but also on the reinforcement type (natural or synthetic fibers) and lay-up sequence [63]. The manufacturing process is affected by residual stresses, and, because it can control the fiber orientation distribution through the flow of material inside the mould, the movement depends on the availability of mix movement due to changes in the mould boundaries. The process parameters modify the cohesion that develops between the matrix and the reinforcing fibers due to the combinations of speed, temperature, and time that are generated in the processes between the material and the final component. Figure 4 shows the manufacturing process for the composites. When the reinforcement is generated by dispersed fibers, the manufacturing process does not have much effect; however, when short or long fibers are used, the process has an effect because the same characteristics modify the flow of the fibers in the matrix, either by injection or compression moulding.

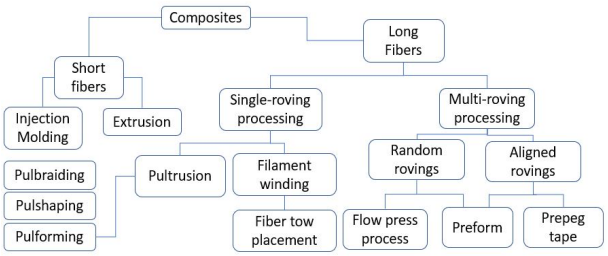


Figure 4. Manufacturing processes for composites.

There are two ways to analyze a load time history: the time domain and the frequency domain. Figure 5 shows both domains for the same time history. Durability assessment can be performed on both domains, and the time domain can be used to reproduce the multiaxial state of loads or to apply a critical load, e.g., at maximum displacement, considering the degrees of freedom of all the loads. The frequency domain is used for the accelerated fatigue test using the power spectral density (energy at different frequencies). In both cases, environmental conditions can be reproduced to improve the fatigue life prediction [38].

The loads generate a time history that must be analyzed to understand the statistics. The main effect is the number of repetitions to which a load is subjected at a certain amplitude. However, there are low amplitudes that are omitted because, by themselves, they do not cause damage, but when applied to a component that has previous damage they can help propagate the fault. The shape of the load and the velocity at which it is applied are analyzed through the waveform and the frequency of the load. Figure 6 shows a schematic waveform. The waveform statistical characteristics are defined by the stress amplitude (S_a). The total range from the minimum load (S_{min}) to the maximum load (S_{max}) per cycle is expressed as S_R:

$$S_R = S_{max} - S_{min} \quad (1)$$

$$S_a = \frac{S_R}{2} = \frac{S_{max} - S_{min}}{2} \quad (2)$$

The mean stress (S_m) is expressed by the mean value of the maximum and minimum loads:

$$S_m = \frac{S_{max} + S_{min}}{2} \quad (3)$$

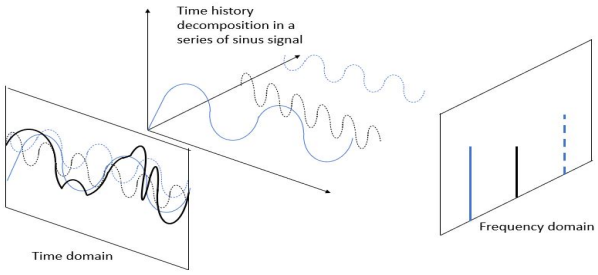


Figure 5. Time signal in the time and frequency domains.

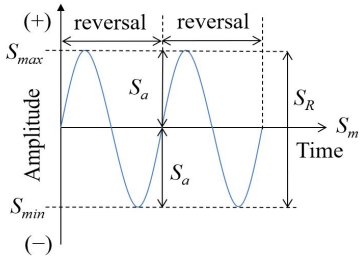


Figure 6. Signal characteristics, adapted from [64].

The fatigue damage process is modified by the mean stress and the different relationships that have different loads. It is defined as the ratio of the minimum to maximum stress ($R = S_{min}/S_{max}$). When $R \geq 0$, the loads open microcracks, accelerating their propagation, while, when $R = \infty$ or $R > 1$, the load relationships tend to compress and close microcracks, which is beneficial for mechanical fatigue. Figure 7 shows different stress ratios.

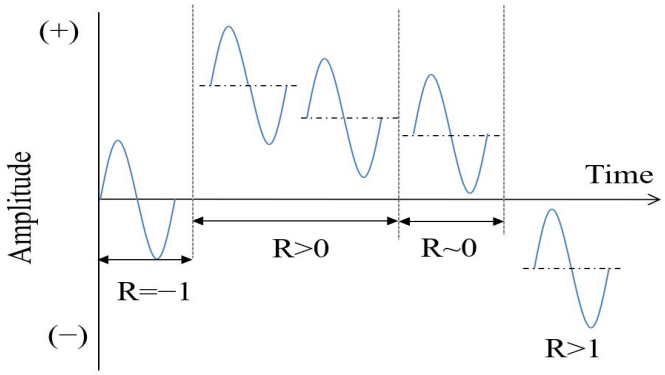
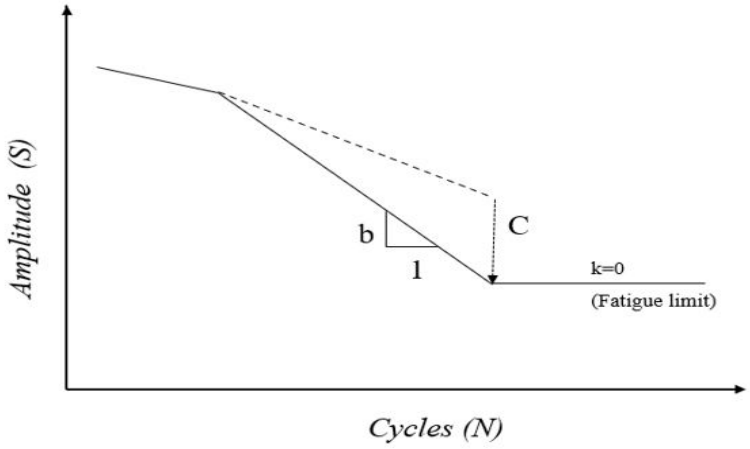


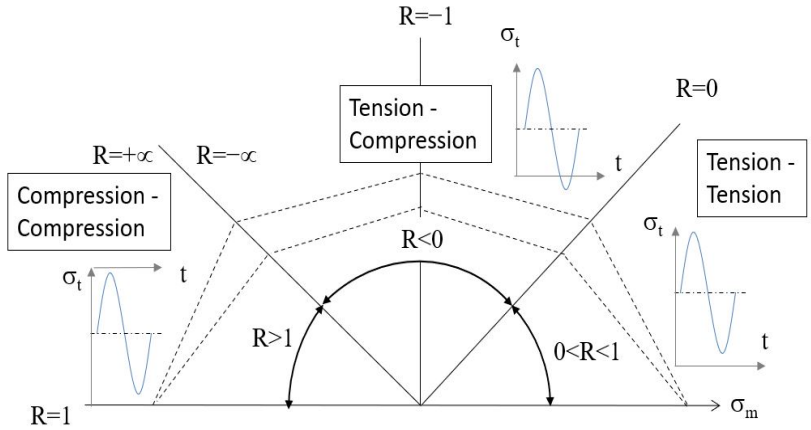
Figure 7. Different stress ratios, adapted from [64].

The cyclic strength is expressed by comparing the amplitudes of the loads (S) and their expected life (N) for the ith load level. The S–N curve cannot be used to generalize the dynamic strength per se. It is necessary to consider factors (C) such as the type of load, surface roughness, and reliability. Although a fatigue limit (at the design stage) has been used, under real-life conditions, failure occurs in the very-high-cycle regime because the high amount of reversal required for failure is necessary for high-frequency test equipment. The failure of components is reached after an expected life and normally occurs outside the guarantee period. Figure 8 shows the fatigue strength of the material using the S–N

curve at different amplitudes (Figure 8a) or at different relationships between the minimum and maximum loads (Figure 8b). Composite materials are sensitive to the relationship between the minimum and maximum loads because this generates different behaviors during tension–compression, tension–tension, or compression–compression. This is due to the behavior of the fibers and depends on the characteristics of the reinforcement because there is a direct effect of the alignment of the fibers on the direction of the load.



(**a**)

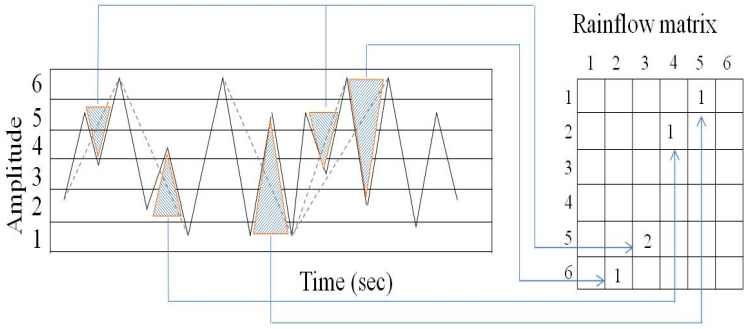


(**b**)

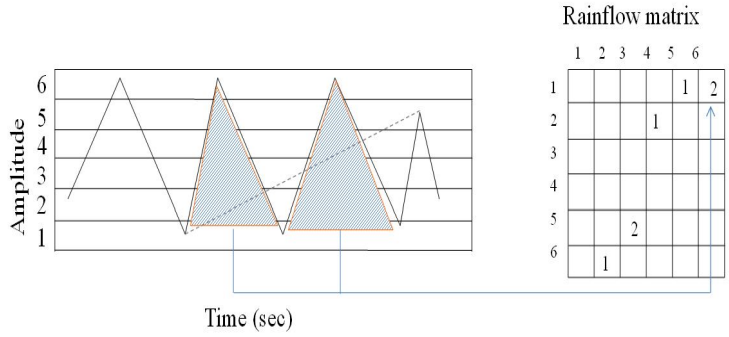
Figure 8. Fatigue strength curves: (**a**) S–N curve and (**b**) stress ratio effect on fatigue, adapted from [65].

The loads are evaluated through statistical analysis using cycle counting processes, which are used to define a summary of the loads generated by load time histories. Rainflow is used to analyze cycles from different time histories. Figure 9a shows the Rainflow cycle counting process as a function of the defined load levels. After every counting, the signal is simplified (Figure 9b) for a new counting process, and the process is repeated until a residue is reached (Figure 9c).

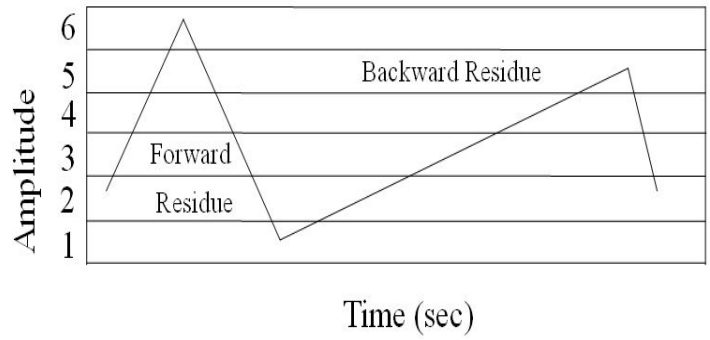
The goal is to define the number of repetitions that the load crosses a specific amplitude; another way to perform cycle counting is level crossing. Considering the load slope, the signal is split at different ranges, and the tendency of one crossing point to the next crossing point is evaluated. When a change is detected, the maximum value is counted, as shown in Figure 10.



(**a**)

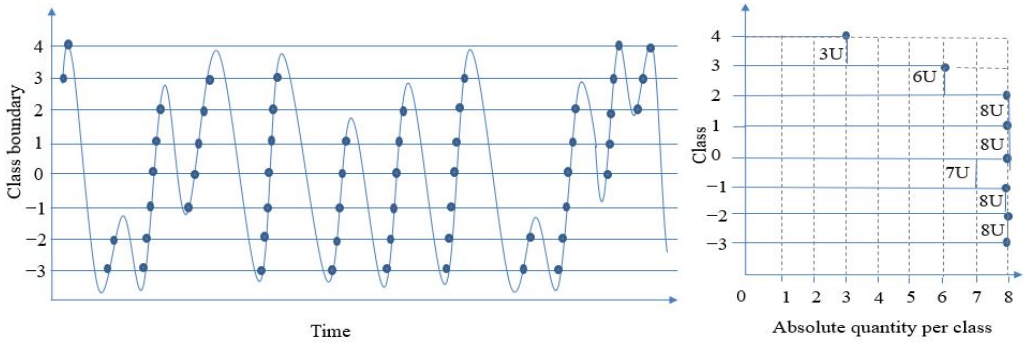


(**b**)



(**c**)

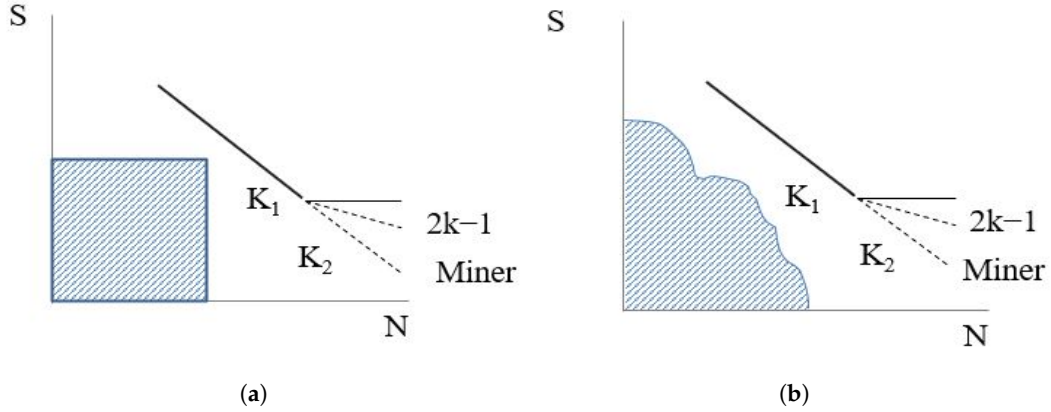
Figure 9. Rainflow counting process: (**a**) initial time history, (**b**) simplified signal, and (**c**) simplified signal residue, adapted from [64].



(**a**) (**b**)

Figure 10. Statistical counting of level crossings: (**a**) load history and (**b**) crossing levels, adapted from [64].

After the counting process is performed with the time histories, the spectrum is defined, as shown in Figure 11. Figure 11a shows a linear spectrum for a constant amplitude load (Figure 11b). In the case of variable amplitude loads, the cycle counting generates a curve (Figure 11b), which represents the number of repetitions and different amplitudes. This spectrum is the basis for comparing a critical value (nearest to the S–N curve, the same material slope). For constant amplitude, the load amplitude (*Sc*) is used, whereas for variable amplitude the critical value is used, and the whole spectrum can be simplified with different amplitude loads (*Si*). This definition makes it possible to generate the life curve of the component, and the dispersion factors must be considered to reduce the probability of failure.



(**a**) (**b**)

Figure 11. Spectra and their relationships with the S–N curve: (**a**) constant amplitude and (**b**) variable amplitude, adapted from [64].

The failure of the composites can be attributed to propagation in the matrix or in the fibers, as shown in Figure 12. This is generated by the accumulation process [58,66,67]. The damage generated in the components is an accumulated process derived from the number of load repetitions and the material strength under dynamic loads. Each repetition within the load history generates material degradation. The way to fail depends on the characteristics of the material; in the case of metals, most of the percentage life by fatigue is for nucleate failure, normally a crack that grows up to a critical size or a sudden failure. In composite materials, the origin and propagation of the failure will depend on the accumulated damage process. However, the failure of composite materials can originate and nucleate both in the base material (matrix) and in the reinforcing fibers. In the case of fiber failure, the material can break or bend. However, failure can also occur by a separation of the materials by having a interlaminar/intralaminar delamination, or in the transition zone.

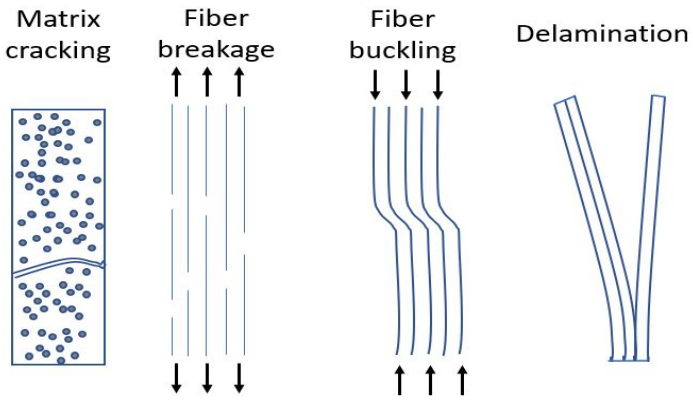


Figure 12. Composite failures.

The stiffness of some composites decreases as a function of the applied cyclic load, and a softer component is generated as a function of the fatigue life, which generates a residual strength that can be used to locate and extend damage, as shown in Figure 13 [68]. In contrast, in metals, fault nucleation develops throughout most of the life of the component. For composite materials, the fault is nucleated in the first stage, and over the course of life faults begin to develop in the matrix and/or the interface through delamination. This growth is gradual and is where a decrease in the strength of the component occurs. In the last stage, the reinforcing fibers fail, and the critical failure of the component is reached.

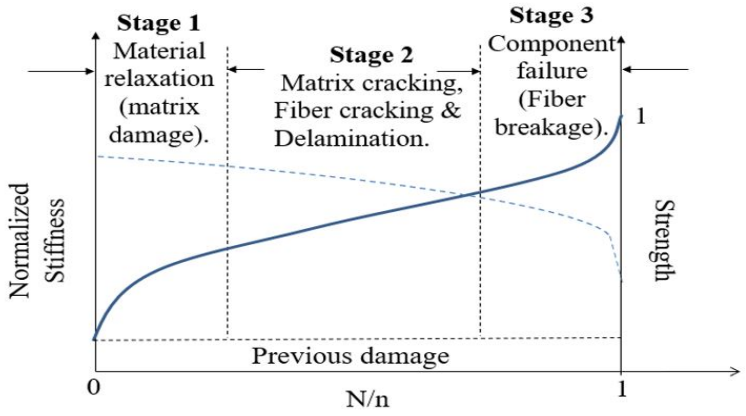


Figure 13. Schematic degradation of the composite strength during fatigue.

The evolution of the damage (Dn) can be evaluated using a relationship between the initial stiffness (Eo), the stiffness at failure (Ef), and the stiffness at the nth cycle (E_n), which depends on the mechanical behavior of the matrix and the reinforcement [69]. It is expressed as follows:

$$D_n = \frac{E_o - E_n}{E_o - E_f} \tag{4}$$

Fatigue behavior is a nonreversible damage process under cyclic loading. The failure can be evaluated using the thermal response, as shown in Figure 14, where in uniaxial fatigue tests the temperature increases until failure. Temperature is directly related to the accumulated damage process; this is because the applied loads generate mechanical energy, resulting in thermal energy. Although there is an increase in temperature due to the speed or frequency of the loads, this must avoid modifying the internal energy of the system, since the increase in temperature is an indicator of the evolution of the damage. The temperature to define a critical failure must be evaluated experimentally, since it depends on several factors such as the amplitude and characteristics of the load, the frequency or frequency range of the load spectrum, and the characteristics of the material [70,71].

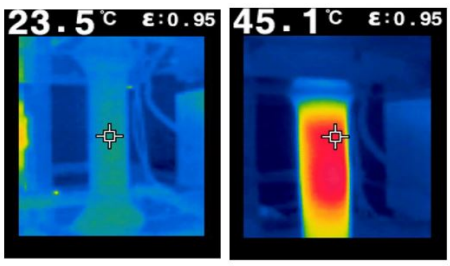


Figure 14. Temperature evolution by accumulated damage for mechanical fatigue, adapted from [70].

The degradation of fiber strength follows a linear degradation per cycle, as in metals expressed by beach marks or chevron patterns. The residual strength (R^r_{II}) depends on the strength of the fiber residual strength (R^s_u) [72] and is expressed as follows:

$$R_{II}^{r} = R_{u}^{s} - \sum_{i=1}^{m} (R_{II}^{s} - \sigma_{max}) \frac{\Delta n_i}{N_f \sigma_{max}} \tag{5}$$

The residual stiffness of composite materials can be defined as the relationship between the fatigue modulus (E) and the strain at the n_{th} cycle [67]:

$$E(n) = \frac{\sigma_{max}}{\varepsilon(n)} = \frac{q\sigma_{ult}}{\varepsilon(n)} \tag{6}$$

The critical damage ($D(n_i)$) is defined as the damage index of failure:

$$D(n_i) = \left(\frac{n_i + n_{i,i-1}^{\frac{log\sigma_i}{log\sigma_{i-1}}}}{N_i} \right)^{\frac{q_w(1-R)}{p_w}} \tag{7}$$

$$n_{i,i-1} = N_i \left(\frac{sinq_{i-1} X_{i-1} cos(q_{i-1} - p_{i-1})}{sinq_{i-1} cos(q_{i-1} X_{i-1} - p_{i-1}} \right)^{n_{i,i-1}} \tag{8}$$

where $X_{i-1} = n_{i-1}/N_{i-1}$, and p_w and q_w are weighted parameters defined by

$$p_w = \frac{\sigma_{min}}{\sigma_{max}} \left(\sqrt{p_{i-1} + p_i} \right) \tag{9}$$

$$q_w = \sqrt{q_{i-1} + q_i} \tag{10}$$

The stress on the fiber orientation (σ_{11}) and its residual strength (X_r) is considered. τ_{12} and S_r are the shear stress and its residual strength, respectively. The fiber failure can be expressed as follows

$$\frac{\sigma_{11}^2}{X_r^2} + \frac{\tau_{12}^2}{S_r} = 1 \tag{11}$$

In multidirectional laminates, the fiber nucleates the failure at 0° plies, so the shear effect can be simplified to

$$\frac{\sigma_{11}^2}{X_r^2} = 1 \tag{12}$$

Considering the principal stress in the transverse direction (σ_{22}) and its residual strength (Y_r), the failure of the matrix can be expressed as follows [73]:

$$\frac{\sigma_{22}^2}{Y_r^2} + \frac{\tau_{12}^2}{S_r} = 1 \tag{13}$$

The average stress and strain relations are

$$\varepsilon_{12}^{*} = C_{12}^{*} \sigma_{12} \tag{14}$$

$$\sigma_{12}^{*} = S_{12}^{*} \sigma_{12} \tag{15}$$

where ε_{12}^{*} is the transformation strain or eigenstrain, and σ_{12}^{*} is the uniform stress. C_{12}^{*} and S_{12}^{*} are the effective stiffness and compliance tensor, respectively, described as follows:

$$S_{ij}^{*} = \left(V_m S_{ik}^{m} + V_k S_{ip}^{f} H_{pk} \right) \left(V_m I_{kj} + V_f H_{kj} \right)^{-1} \tag{16}$$

$$C_{ij}^{*} = \left(V_m C_{ik}^{m} + V_f C_{ip}^{f} T_{pk} \right) \left(V_m I_{kj} + V_f T_{kj} \right)^{-1} \tag{17}$$

where V_f and V_m are the volume fractions of the fibers and matrix, respectively. I_{ij} is the second-order unit tensor. T_{ij} and H_{ij} can be obtained [74]

$$T_{ij} = \left[I_{ij} + K_{ik} S^m_{kp} (C^f_{pj} - C^m_{pj}) \right]^{-1} \tag{18}$$

$$H_{ij} = C^f_{ik} T_{kp} S^m_{pj} = C^f_{ik} \left[I_{kq} + K_{kl} S^m_{lp} (C^f_{pq} - C^m_{pq}) \right]^{-1} S^m_{qj} \tag{19}$$

The fiber failure modes are expressed for $\sigma_1 > 0$:

$$\frac{\sigma_1}{X_t} - \nu_{12} \frac{\sigma_2}{X_t} + \nu_{f12} \frac{E_1}{E_2} \cdot m_{\sigma f} \frac{\sigma_2}{X_t} = 1 \tag{20}$$

and for $\sigma_1 < 0$

$$\left| \frac{\sigma_1}{X_t} - \nu_{12} \frac{\sigma_2}{X_t} + \nu_{f12} \frac{E_1}{E_2} \cdot m_{\sigma f} \frac{\sigma_2}{X_t} \right| + (10\gamma_{12})^2 = 1 \tag{21}$$

where X is the strength of the lamina under tension (t) and compression (c), respectively. The subscript f denotes the fiber properties [75,76].

4. Neural Networks in Fatigue Life Prediction

Structural degradation by mechanical fatigue has been studied for several years; however, this topic is not fully understood, and damage models are not sufficiently accurate because of the complexity of the materials [77], loads and manufacturing process [78]. Machine learning algorithms, such as artificial neural networks, random forests, and deep learning, have been used not only to emulate and predict physical behavior as material properties [79–81] but also for determining loads and uncertainties [82–84] or fatigue life in different materials, such as elastomers [85] and titanium [79,86,87]. Its learning capabilities can include defects in the training stage [88,89], which can be generated during the manufacturing process or for abuse due to random events [58,90–92].

The mechanism of failure depends on the stacking sequence for damage nucleation and propagation [93]. Noninvasive methods can be used to analyze the mechanical response. The modal response is an acoustic response in which changes in the microstructure modify the response [66,94,95] or the power spectral density [96]. The training models can be based on raw data or virtual data using finite element analysis and machine learning models [97–100]. These models improve the efficiency of structural health monitoring by relating the mechanical strength, the raw data and the fatigue models [101,102].

Damage detection on structures can be performed using deep learning, which analyzes the nonlinear behavior of plastic components reinforced with carbon fibers. However, some analyses, such as those performed as black boxes and to improve the prediction with a limited amount of information, are necessary to feed the network with the phenomenon-related physics, not only to reduce the expense of the training process but also to help the model predict the behavior. Fatigue damage-based stiffness degradation can be used as an input to the network to determine the relationships between and among different layers, using changes in the response as eigenvalues, time history, or frequency information using power spectral density [96,103]. Zhang and Gu proposed a machine learning model for developing composite materials through digital simulations using the minimum energy criterion as the loss function [104]. A physics-informed neural network has also been used to predict fatigue life under a multiaxial load state [105].

Machine learning, founded on statistical principles, can be employed to predict the dynamic behavior of mechanical phenomena, utilizing both raw and synthetic data for training. This information must be used to train and validate numerical models. In the case with a series of actions that are required for a final prediction, reinforcement learning is used. The characteristics of the network include neurons, the algorithm that determines how the information is processed, and the topology to integrate new numerical models through different layers from the input, analysis (hidden layers), and output layers. Neurons are

connected internally and externally to transfer information and connect the previous stage to the next stage (Figure 15).

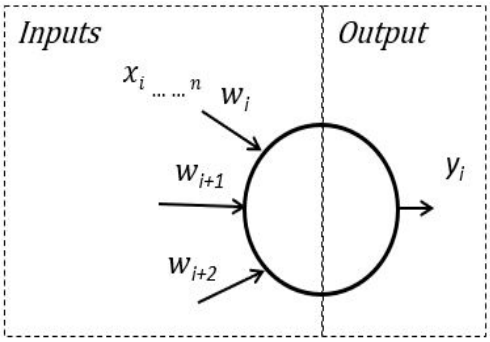


Figure 15. Model of a single neuron.

There is a relationship between a pair of neurons; this relation is the weighting coefficient that depends on the physics development, and it affects the process of obtaining different weights (w). It can strengthen or weaken the output of a neuron. The input (I_i) to a neuron is expressed by

$$I_i = \sum_{j=1}^{n} x_j w_{ij} \tag{22}$$

A neuron cannot produce an output until it has a trigger, when the total input exceeds a threshold (θ_i), defined by

$$s_i = \sum_{j=1}^{n} x_j w_{ij} - \theta_i \tag{23}$$

The active value of a neuron, considering a continuous function (g), is $u_i = g(s_i)$. The output of a neuron is defined by

$$y_i = f(u_i) = f\left(\sum_{j=1}^{n} x_j w_{ij} - \theta_i\right) \tag{24}$$

where f is the activation function. Although the most commonly used activation function is the S form, expressed mathematically by the sigmoid function, the ramp and step functions can also be used [106].

$$f(u) = \frac{1}{1 + e^{-u}} \tag{25}$$

The connection between layers is not direct between the input and output; there are hidden layers with different configurations depending on the main target.

Although it has the ability to reproduce the relationships of complex nonlinear systems to predict the behavior of the output as a function of the inputs, the interconnection between the different layers modifies the relative weights between the different neurons, and the architecture has an effect on how this information moves to the next layer, as is shown in Figure 16. Once the network topology is defined, the relationships between the neurons are adjusted by training to learn and minimize the output error, which is performed in an iterative process until it is below a specific target. This process uses weighting adjustments and defines the proportion that propagates to the error. Back propagation networks are based on this process.

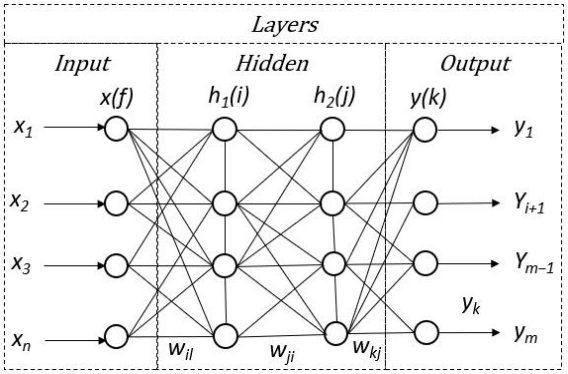


Figure 16. Multilayer network with two hidden layers.

The error at the output layer depends on the expected output (t_k) and the output node (O_k), expressed by

$$\delta k = (t_k - O_k)O_k(1 - O_k) \tag{26}$$

where $O_k(1 - O_k)$ is the derivative of the trigger function. The weights ($\omega_{j,k}$) are functions of the error at node k times the activation node (j), including the learning rate (l_r), and the change in the weight ($\Delta W_{j,k}$) is defined by

$$\Delta W_{j,k} = l_r \delta_k X_k \tag{27}$$

The error at the hidden layer and the updating weight ($\Delta W_{j,k}^n$) are summarized as follows:

$$\Delta W_{j,k} = l_r \delta_k X_k + \Delta W_{j,k}^{n-1} \mu \tag{28}$$

When the error has a tendency to be minimized, $E < \varepsilon$, the learning process is finished. The general training, validation, and testing processes stop the iterative and updating processes.

$$E = \frac{1}{2} \sum \left(\sum (t_k - Ok)^2 \right) \tag{29}$$

To evaluate the performance of the network, the network output is compared against the expected physical or raw response using the root mean square error:

$$RMSE = \sqrt{\frac{1}{N} \sum_{i=1}^{N} (t_i - td_i)^2} \tag{30}$$

Another type of neural network for failure detection is the nonlinear autoregressive exogenous $(NARX)$ model, which, based on its topology that considers previous data using delays, could be useful for nonlinear responses. The topology is shown in Figure 17 and Equation (31).

$$y(t) = f\left[y(t-1), \ldots, y(t-n_y, u(t-1), \ldots, u(t-n_u + e(t)\right] \tag{31}$$

where n_y and u_n are the output and the past input, respectively. The delay units $(z - 1)$ are used to predict the next point on the input layer. The output data are computed using the bipolar sigmoid function (f_1), which is expressed by

$$y_p(t) = f_1 \left(\sum_{i=1}^{K} Iw_i u_i + \sum_{j=1}^{K} Iw_o y_j + b_i \right) \tag{32}$$

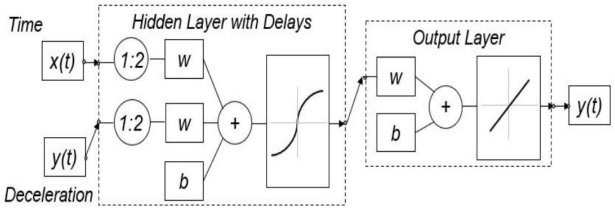


Figure 17. Schematic of the NARX neural network.

The application of artificial intelligence helps predict nonlinear behaviors, such as fatigue life in composite materials. The degradation of materials generates the need to implement numerical processes that allow updating of the behavior of the material. The topology and characteristics of the neural network will depend on the available parameters that can be used as input to predict fatigue life. It is possible to include material characteristics as inputs, which can include chemical composition, and also mechanical properties such as Young's modulus, yield stress, UTS, and strain at fracture. Fatigue can also be predicted directly by the load amplitudes and their characteristics, such as maximum effort, minimum effort, and relationship between efforts. Likewise, numerical models can be included that help the network predict durability; this can be done through nested networks including damage models. By using the results of experimental tests, the results are validated by having a low error percentage.

5. Conclusions

The battery housings of electric cars meet different conditions to protect the batteries from vibrations, impacts, and humidity. This could cause an unwanted battery reaction, but at the same time the housings protect against electromagnetic fields and in the case of fire retard the spread of flames. These loads generate accumulated damage during operation, so predicting the durability of the components is essential to prevent failures throughout the useful life of the vehicle and the battery.

Mechanical fatigue analysis is essential for predicting component failure during operation, particularly for safety-critical systems. While systems or vehicles may continue functioning until a failed component is replaced, the failure of safety systems can lead to significant risks, including damage to the mechanical components and vehicle occupants or pedestrians. Achieving sustainable mobility requires integrating advanced composite materials due to their superior weight-to-strength ratio, making them ideal for reducing vehicle weight while maintaining structural integrity. However, the long-term durability of these materials, especially in electric vehicle battery housings, remains underexplored.

Fatigue prediction in battery housings is crucial for ensuring long-term performance and preventing failures that may compromise the battery system's operation and protective capabilities. Although AI is increasingly used to predict mechanical behavior, challenges remain, particularly in extrapolating predictions over extended lifespans and different load cases. These challenges necessitate extensive experimental testing to account for diverse driving conditions, environmental influences, and vehicle characteristics. Furthermore, AI models are data-intensive, requiring large datasets for training and validation, which presents an additional limitation.

Environmental factors and load changes are significant sources of variability in mechanical fatigue. As a component's strength changes, the load it experiences can shift from a biaxial to a multiaxial stress state, particularly in electric vehicle battery housings. These loads come from various sources, including battery weight, vehicle acceleration forces, thermal loads, road impacts, and environmental factors, contributing to cumulative damage.

Neural networks have shown promise in improving the reliability of fatigue life predictions. However, accurate modeling must incorporate detailed information on material properties, load conditions, and manufacturing processes. Given their complexity, composite materials require precise models that reflect their anisotropic behavior and failure mechanisms, including matrix failure, reinforcement failure, and delamination. Dynamic

models that update material properties based on real-time data are crucial to reducing variability and improving prediction accuracy.

The numerical model to be used to predict mechanical fatigue depends on the amount of information available or relevant to analyze the physical phenomenon. Although there are machine learning techniques that can predict phenomena more accurately, they eventually fall into overfitting because they require a large number of data. Sometimes networks such as the feedforward are better when there are few data, as is the case of mechanical properties such as the life curve (S–N), or few results for the training of the network.

The integration of AI in fatigue life prediction provides an opportunity to optimize the performance of lightweight components. However, AI models must be informed by the underlying physics of the materials rather than being treated as "black boxes". By integrating AI with a physics-based approach, the accuracy of fatigue life predictions can be enhanced, leading to the development of lighter, more efficient components that extend vehicle range, reduce environmental impact, and allow for the recycling of components into systems with lower mechanical strength requirements.

The use of composite materials for the manufacture of battery housing for electric cars allows the development of innovative concepts to achieve the objective of reducing weight. However, an area of opportunity lies in the different recycling processes. Due to their nature, composite materials are difficult to recycle; it is important to consider the material recovery stage at the end of their useful life. Mechanical, chemical, and thermal methods can be implemented to separate the fibers from the matrix. In some cases, the matrix material can be incinerated for energy generation and at the same time the reinforcing fiber can be recovered. However, some of these processes can emit harmful gases, negatively impacting the environment.

Author Contributions: Conceptualisation, M.J.-M.; methodology, M.J.-M.; formal analysis, J.L.V.-S., S.G.T.-C., J.C.-P. and M.J.-M.; investigation, J.L.V.-S. and M.J.-M.; resources, M.J.-M. and J.C.-P.; data curation, J.L.V.-S.; writing—original draft preparation, M.J.-M.; writing—review and editing, M.J.-M. and S.G.T.-C.; supervision, M.J.-M. All authors have read and agreed to the published version of the manuscript.

Funding: This research is partially funded by the Kautex Lightweight structures Lab at Tecnologico de Monterrey Campus Puebla, with the sponsorship of Kautex Textron GmbH.

Data Availability Statement: Data are contained within the article.

Acknowledgments: S.G.T.-C. and J.C.-P. extend their sincere gratitude to the DGAPA-PAPIIT program, grant number IN118920, for the provision of computational resources utilized in this project.

Conflicts of Interest: The authors declare no conflicts of interest.

References

1. Ahmadi, P. Environmental impacts and behavioral drivers of deep decarbonization for transportation through electric vehicles. *J. Clean. Prod.* **2019**, *225*, 1209–1219. [CrossRef]
2. Delogu, M.; Zanchi, L.; Dattilo, C.A.; Pierini, M. Innovative composites and hybrid materials for electric vehicles lightweight design in a sustainability perspective. *Mater. Today Commun.* **2017**, *13*, 192–209. [CrossRef]
3. Machacek, D.T.; Yasar, N.O.; Huber, T.; Onder, C.H. Energy management of hydrogen hybrid electric vehicles—A potential analysis. *Int. J. Hydrogen Energy* **2024**, *58*, 1–13. [CrossRef]
4. Roper, S.W.K.; Kim, I.Y. Integrated topology and packaging optimization for conceptual-level electric vehicle chassis design via the component-existence method. *Proc. Inst. Mech. Eng. Part D J. Automob. Eng.* **2023**, *237*, 2118–2131. [CrossRef]
5. Zhang, S.; Xiong, R.; Cao, J. Battery durability and longevity based power management for plug-in hybrid electric vehicle with hybrid energy storage system. *Appl. Energy* **2016**, *179*, 316–328. [CrossRef]
6. Liu, Y.; Liao, Y.G.; Lai, M.C. Fuel economy improvement and emission reduction of 48 V mild hybrid electric vehicles with P0, P1, and P2 architectures with lithium battery cell experimental data. *Adv. Mech. Eng.* **2021**, *13*, 16878140211036022. [CrossRef]
7. Sabri, M.; Danapalasingam, K.A.; Rahmat, M.F. A review on hybrid electric vehicles architecture and energy management strategies. *Renew. Sustain. Energy Rev.* **2016**, *53*, 1433–1442. [CrossRef]
8. Nabi, M.N.; Ray, B.; Rashid, F.; Al Hussam, W.; Muyeen, S. Parametric analysis and prediction of energy consumption of electric vehicles using machine learning. *J. Energy Storage* **2023**, *72*, 108226. [CrossRef]

9. Veza, I.; Asy'ari, M.Z.; Idris, M.; Epin, V.; Fattah, I.R.; Spraggon, M. Electric vehicle (EV) and driving towards sustainability: Comparison between EV, HEV, PHEV, and ICE vehicles to achieve net zero emissions by 2050 from EV. *Alex. Eng. J.* **2023**, *82*, 459–467. [CrossRef]
10. Boretti, A. The perspective of hybrid electric hydrogen propulsion systems. *Int. J. Hydrogen Energy* **2024**, *50*, 857–868. [CrossRef]
11. Gasco, F.; Feraboli, P. Manufacturability of composite laminates with integrated thin film Li-ion batteries. *J. Compos. Mater.* **2014**, *48*, 899–910. [CrossRef]
12. Wang, W.; Yang, S.; Lin, C.; Shen, W.; Lu, G.; Li, Y.; Zhang, J. Investigation of mechanical property of cylindrical lithium-ion batteries under dynamic loadings. *J. Power Sources* **2020**, *451*, 227749. [CrossRef]
13. Xiong, Y.; Pan, Y.; Wu, L.; Liu, B. Effective weight-reduction-and crashworthiness-analysis of a vehicle's battery-pack system via orthogonal experimental design and response surface methodology. *Eng. Fail. Anal.* **2021**, *128*, 105635. [CrossRef]
14. Taghavifar, H. The influence of different fuels and injection methods of RCCI and DCI in hybrid ICE-Battery vehicle performance. *Fuel* **2023**, *340*, 127467. [CrossRef]
15. Arat, H.T. Alternative fuelled hybrid electric vehicle (AF-HEV) with hydrogen enriched internal combustion engine. *Int. J. Hydrogen Energy* **2019**, *44*, 19005–19016. [CrossRef]
16. Shah, R.; Mittal, V.; Matsil, E.; Rosenkranz, A. Magnesium-ion batteries for electric vehicles: Current trends and future perspectives. *Adv. Mech. Eng.* **2021**, *13*, 16878140211003398. [CrossRef]
17. Pejman, R.; Gorman, J.; Najafi, A.R. Multi-physics design of a new battery packaging for electric vehicles utilizing multifunctional composites. *Compos. Part B Eng.* **2022**, *237*, 109810. [CrossRef]
18. Pan, Y.; Xiong, Y.; Wu, L.; Diao, K.; Guo, W. Lightweight design of an automotive battery-pack enclosure via advanced high-strength steels and size optimization. *Int. J. Automot. Technol.* **2021**, *22*, 1279–1290. [CrossRef]
19. Buidin, T.I.C.; Mariasiu, F. Battery thermal management systems: Current status and design approach of cooling technologies. *Energies* **2021**, *14*, 4879. [CrossRef]
20. Li, W.; Zhou, Y.; Zhang, H.; Tang, X. A review on battery thermal management for new energy vehicles. *Energies* **2023**, *16*, 4845. [CrossRef]
21. Chan, C.K.; Chung, C.H.; Raman, J. Optimizing Thermal Management System in Electric Vehicle Battery Packs for Sustainable Transportation. *Sustainability* **2023**, *15*, 11822. [CrossRef]
22. Chen, K.; Yang, L.; Chen, Y.; Wu, B.; Song, M. Efficient Design of Battery Thermal Management Systems for Improving Cooling Performance and Reducing Pressure Drop. *Energies* **2024**, *17*, 2275. [CrossRef]
23. Zhang, F.; Zhai, L.; Zhang, L.; Yi, M.; Du, B.; Li, S. A novel hybrid battery thermal management system with fins added on and between liquid cooling channels in composite phase change materials. *Appl. Therm. Eng.* **2022**, *207*, 118198. [CrossRef]
24. Deng, J.; Huang, Q.; Li, X.; Zhang, G.; Li, C.; Li, S. Influence mechanism of battery thermal management with flexible flame retardant composite phase change materials by temperature aging. *Renew. Energy* **2024**, *222*, 119922. [CrossRef]
25. Huang, Y.H.; Cheng, W.L.; Zhao, R. Thermal management of Li-ion battery pack with the application of flexible form-stable composite phase change materials. *Energy Convers. Manag.* **2019**, *182*, 9–20. [CrossRef]
26. Tang, Z.; Feng, R.; Huang, P.; Bai, Z.; Wang, Q. Modeling analysis on the cooling efficiency of composite phase change material-heat pipe coupling system in battery pack. *J. Loss Prev. Process Ind.* **2022**, *78*, 104829. [CrossRef]
27. Luo, J.; Zou, D.; Wang, Y.; Wang, S.; Huang, L. Battery thermal management systems (BTMs) based on phase change material (PCM): A comprehensive review. *Chem. Eng. J.* **2022**, *430*, 132741. [CrossRef]
28. Zhang, J.; Li, X.; Zhang, G.; Wu, H.; Rao, Z.; Guo, J.; Zhou, D. Experimental investigation of the flame retardant and form-stable composite phase change materials for a power battery thermal management system. *J. Power Sources* **2020**, *480*, 229116. [CrossRef]
29. Sun, Z.; Guo, Y.; Zhang, C.; Whitehouse, J.; Zhou, Q.; Xu, H.; Wang, C. Experimental study of battery passive thermal management system using copper foam-based phase change materials. *Int. J. Thermofluids* **2023**, *17*, 100255. [CrossRef]
30. Schmolke, T.; Teutenberg, D.; Meschut, G. Development of a test method for investigating the leak tightness of hybrid joined battery housing connections. *Int. J. Adhes. Adhes.* **2022**, *117*, 103171. [CrossRef]
31. Arora, S.; Shen, W.; Kapoor, A. Review of mechanical design and strategic placement technique of a robust battery pack for electric vehicles. *Renew. Sustain. Energy Rev.* **2016**, *60*, 1319–1331. [CrossRef]
32. Lee, P.Y.; Park, S.; Cho, I.; Kim, J. Vibration-based degradation effect in rechargeable lithium ion batteries having different cathode materials for railway vehicle application. *Eng. Fail. Anal.* **2021**, *124*, 105334. [CrossRef]
33. Shui, L.; Chen, F.; Garg, A.; Peng, X.; Bao, N.; Zhang, J. Design optimization of battery pack enclosure for electric vehicle. *Struct. Multidiscip. Optim.* **2018**, *58*, 331–347. [CrossRef]
34. Li, H.; Peng, W.; Yang, X.; Chen, H.; Sun, J.; Wang, Q. Full-Scale Experimental Study on the Combustion Behavior of Lithium Ion Battery Pack Used for Electric Vehicle. *Fire Technol.* **2020**, *56*, 2545–2564. [CrossRef]
35. Zhu, J.; Wierzbicki, T.; Li, W. A review of safety-focused mechanical modeling of commercial lithium-ion batteries. *J. Power Sources* **2018**, *378*, 153–168. [CrossRef]
36. Zhang, X.; Xiong, Y.; Pan, Y.; Du, H.; Liu, B. Crushing stress and vibration fatigue-life optimization of a battery-pack system. *Struct. Multidiscip. Optim.* **2023**, *66*, 48. [CrossRef]
37. Wang, W.; Dai, S.; Zhao, W.; Wang, C.; Ma, T. Design optimization of a novel negative Poisson's ratio non-module battery pack system considering crashworthiness and heat dissipation. *Compos. Struct.* **2021**, *275*, 114458. [CrossRef]

38. Yang, Y.; Xu, X.; Zhang, Y.; Hu, H.; Li, C. Synergy analysis on the heat dissipation performance of a battery pack under air cooling. *Ionics* **2020**, *26*, 5575–5584. [CrossRef]
39. Krüger, C.; Spohr, S.; Merdivan, D.; Urban, P. Avoiding structural redundancies between the vehicle body and the battery housing based on a functional integration approach. *Automot. Engine Technol.* **2022**, *7*, 197–208. [CrossRef]
40. Xu, C.; Weng, L.; Ji, L.; Zhou, J. An analytical model for the fracture behavior of the flexible lithium-ion batteries under bending deformation. *Eur. J. Mech.-A/Solids* **2019**, *73*, 47–56. [CrossRef]
41. Yang, Y.; Boom, R.; Irion, B.; van Heerden, D.J.; Kuiper, P.; de Wit, H. Recycling of composite materials. *Chem. Eng. Process. Process Intensif.* **2012**, *51*, 53–68 [CrossRef]
42. Coren, F.; Stelzer, P.S.; Reinbacher, D.; Ellersdorfer, C.; Fischer, P.; Major, Z. Dynamic failure and crash simulation of carbon fiber sheet moulding compound (CF-SMC). *Automot. Engine Technol.* **2021**, *6*, 63–77. [CrossRef]
43. Schuh, G.; Bergweiler, G.; Fiedler, F.; Koltermann, M. Flexible Production Concept of a Low-Cost Battery Pack Housing for Electric Vehicles. In Proceedings of the 53rd CIRP Conference on Manufacturing Systems 2020, Chicago, IL, USA, 1–3 July 2020; Volume 93, pp. 137–142.
44. Sglcarbon. Battery Cases for Electric Cars. Available online: https://www.sglcarbon.com/en/markets-solutions/applications/battery-cases/# (accessed on 3 July 2024).
45. Kautex. Pentatonic Battery Enclosures. Available online: https://www.kautex.com/en/mobility/battery-enclosures (accessed on 3 July 2024).
46. Syensqo. Battery Pack. Available online: https://www.syensqo.com/en/solutions-market/batteries/battery-pack (accessed on 3 July 2024).
47. Plasticstoday. Composites Drive Battery Lightweighting in EVs. Available online: https://www.plasticstoday.com/automotive-mobility/composites-drive-battery-lightweighting-in-evs (accessed on 3 July 2024).
48. IDTechEx. Materials for Electric Vehicle Battery Cells and Packs 2023–2033. Available online: https://www.idtechex.com/en/research-report/materials-for-electric-vehicle-battery-cells-and-packs-2023-2033/936 (accessed on 3 July 2024).
49. BCP. Composite Panel Solutions for Electric Vehicle Battery Systems. Available online: https://bespokecompositepanels.com/sectors/ev-battery-housing-plate/ (accessed on 3 July 2024).
50. Huntsman. Battery Housing. Available online: https://www.huntsman-transportation.com/EN/applications/applications-for-composites/battery-housing.html (accessed on 3 July 2024).
51. Gültekin, E.; Yahşi, M. Dynamic compression and impact analyses of the lattice structures for battery safety. *Proc. Inst. Mech. Eng. Part D J. Automob. Eng.* **2023**, *237*, 930–940.
52. Höhne, C.C.; Blaess, P.; Ilinzeer, S.; Griesbaum, P. New approach for electric vehicle composite battery housings: Electromagnetic shielding and flame retardancy of PUR/UP-based sheet moulding compound. *Compos. Part A Appl. Sci. Manuf.* **2023**, *167*, 107404.
53. Kwon, Y.I.; Lim, E.; Song, Y.S. Simulation of injection-compression molding for thin and large battery housing. *Curr. Appl. Phys.* **2018**, *18*, 1451–1457.
54. Lee, S.; Shin, D.; Kim, G.; Ji, W. Numerical model for compression molding process of hybridly laminated thermoplastic composites based on anisotropic rheology. *Compos. Part C Open Access* **2022**, *7*, 100215. [CrossRef]
55. Shan, L.; Tan, C.; Shen, X.; Ramesh, S.; Zarei, M.; Kolahchi, R.; Hajmohammad, M. The effects of nano-additives on the mechanical, impact, vibration, and buckling/post-buckling properties of composites: A review. *J. Mater. Res. Technol.* **2023**, *24*, 7570–7598. [CrossRef]
56. Lizama-Camara, Y.; Pinna, C.; Lu, Z.; Blagdon, M. Effect of the injection moulding fibre orientation distribution on the fatigue life of short glass fibre reinforced plastics for automotive applications. *Procedia CIRP* **2019**, *85*, 255–260. [CrossRef]
57. Carraro, P.A.; Maragoni, L.; Quaresimin, M. Characterisation and analysis of transverse crack-induced delamination in cross-ply composite laminates under fatigue loadings. *Int. J. Fatigue* **2019**, *129*, 105217. [CrossRef]
58. Zhou, T.; Jiang, S.; Han, T.; Zhu, S.P.; Cai, Y. A physically consistent framework for fatigue life prediction using probabilistic physics-informed neural network. *Int. J. Fatigue* **2023**, *166*, 107234. [CrossRef]
59. Halamka, J.; Bartošák, M.; Španiel, M. Using hybrid physics-informed neural networks to predict lifetime under multiaxial fatigue loading. *Eng. Fract. Mech.* **2023**, *289*, 109351. [CrossRef]
60. Guo, Y.E.; Shang, D.G.; Cai, D.; Jin, T.; Li, D.H. Fatigue life prediction considering temperature effect for carbon fibre reinforced composites under variable amplitude loading. *Int. J. Fatigue* **2023**, *168*, 107442. [CrossRef]
61. Tao, C.; Qiu, J.; Yao, W.; Ji, H. A novel method for fatigue delamination simulation in composite laminates. *Compos. Sci. Technol.* **2016**, *128*, 104–115. [CrossRef]
62. Kulkarni, S.S.; Hale, F.; Taufique, M.; Soulami, A.; Devanathan, R. Investigation of Crashworthiness of Carbon Fiber-Based Electric Vehicle Battery Enclosure Using Finite Element Analysis. *Appl. Compos. Mater.* **2023**, *30*, 1689–1715. [CrossRef]
63. Rajiv, B.; Kalos, P.; Pantawane, P.; Chougule, V.; Chavan, V. Classification of damages in composite material using multi-support vector machine. *J. Inst. Eng. (India) Ser. C* **2022**, *103*, 655–661. [CrossRef]
64. Jimenez, M. Accelerated fatigue test in mechanical components. In *Contact and Fracture Mechanics*; IntechOpen: London, UK, 2018; pp. 253–273.
65. Harris, B. *Fatigue in Composites: Science and Technology of the Fatigue Response of Fibre-Reinforced Plastics*; CRC Press LLC: Boca Raton, FL, USA, 2003.

66. Zhang, B.; Shi, D.; Liu, C.; Hao, W.; Yang, X. Physics-informed machine learning with high-throughput design module for evaluating rupture life and guiding design of oxide/oxide ceramic matrix composites. *Ceram. Int.* **2023**, *49*, 34945–34957. [CrossRef]
67. Zhao, L.; Shan, M.; Hong, H.; Qi, D.; Zhang, J.; Hu, N. A residual strain model for progressive fatigue damage analysis of composite structures. *Compos. Struct.* **2017**, *169*, 69–78. [CrossRef]
68. D'Amore, A.; Grassia, L. Phenomenological approach to the study of hierarchical damage mechanisms in composite materials subjected to fatigue loadings. *Compos. Struct.* **2017**, *175*, 1–6. [CrossRef]
69. Suzuki, T.; Mahfuz, H.; Takanashi, M. A new stiffness degradation model for fatigue life prediction of GFRPs under random loading. *Int. J. Fatigue* **2019**, *119*, 220–228. [CrossRef]
70. Jimenez-Martinez, M.; Varela-Soriano, J.; De La Trinidad-Rendon, J.S.; Torres-Cedillo, S.G.; Cortés-Pérez, J.; Coca-Gonzalez, M. Fatigue Analysis of Printed Composites of Onyx and Kevlar. *J. Compos. Sci.* **2023**, *8*, 12. [CrossRef]
71. Niaki, S.A.; Haghighat, E.; Campbell, T.; Poursartip, A.; Vaziri, R. Physics-informed neural network for modelling the thermo-chemical curing process of composite-tool systems during manufacture. *Comput. Methods Appl. Mech. Eng.* **2021**, *384*, 113959. [CrossRef]
72. Kennedy, C.R.; Brádaigh, C.M.Ó.; Leen, S.B. A multiaxial fatigue damage model for fibre reinforced polymer composites. *Compos. Struct.* **2013**, *106*, 201–210. [CrossRef]
73. Lian, W.; Yao, W. Fatigue life prediction of composite laminates by FEA simulation method. *Int. J. Fatigue* **2010**, *32*, 123–133. [CrossRef]
74. Mohammadi, B.; Shokrieh, M.; Jamali, M.; Mahmoudi, A.; Fazlali, B. Damage-entropy model for fatigue life evaluation of off-axis unidirectional composites. *Compos. Struct.* **2021**, *270*, 114100. [CrossRef]
75. Dong, H.; Li, Z.; Wang, J.; Karihaloo, B. A new fatigue failure theory for multidirectional fiber-reinforced composite laminates with arbitrary stacking sequence. *Int. J. Fatigue* **2016**, *87*, 294–300. [CrossRef]
76. Llobet, J.; Maimí, P.; Mayugo, J.; Essa, Y.; de la Escalera, F.M. A fatigue damage and residual strength model for unidirectional carbon/epoxy composites under on-axis tension-tension loadings. *Int. J. Fatigue* **2017**, *103*, 508–515. [CrossRef]
77. Liu, C.; Xu, X.; Wu, J.; Zhu, H.; Wang, C. Deep transfer learning-based damage detection of composite structures by fusing monitoring data with physical mechanism. *Eng. Appl. Artif. Intell.* **2023**, *123*, 106245. [CrossRef]
78. Plets, J.; Bouckaert, Q.; Ahmed, B.; De Waele, W.; Hectors, K. Neural network based fatigue lifetime prediction of metals subjected to block loading. *Int. J. Fatigue* **2024**, *183*, 108283. [CrossRef]
79. Oliveira, G.A.B.; Cardoso, R.A.; Júnior, R.C.S.F.; Doca, T.; Araújo, J.A. On the generalization capability of artificial neural networks used to estimate fretting fatigue life. *Tribol. Int.* **2024**, *192*, 109222. [CrossRef]
80. Gao, J.; Heng, F.; Yuan, Y.; Liu, Y. A novel machine learning method for multiaxial fatigue life prediction: Improved adaptive neuro-fuzzy inference system. *Int. J. Fatigue* **2024**, *178*, 108007. [CrossRef]
81. Tao, C.; Zhang, C.; Hongli, J.; Qiu, J. Neural cohesive model for delamination simulation in composite laminates under cyclic loadings. *Int. J. Fatigue* **2022**, *164*, 107123. [CrossRef]
82. Baisthakur, S.; Fitzgerald, B. Physics-Informed Neural Network surrogate model for bypassing Blade Element Momentum theory in wind turbine aerodynamic load estimation. *Renew. Energy* **2024**, *224*, 120122. [CrossRef]
83. Fernández, J.; Chiachío, J.; Barros, J.; Chiachío, M.; Kulkarni, C.S. Physics-guided recurrent neural network trained with approximate Bayesian computation: A case study on structural response prognostics. *Reliab. Eng. Syst. Saf.* **2024**, *243*, 109822. [CrossRef]
84. He, G.; Zhao, Y.; Yan, C. Uncertainty quantification in multiaxial fatigue life prediction using Bayesian neural networks. *Eng. Fract. Mech.* **2024**, *298*, 109961. [CrossRef]
85. Li, C.; Yang, H.; Suo, Z.; Tang, J. Fatigue-Resistant elastomers. *J. Mech. Phys. Solids* **2020**, *134*, 103751. [CrossRef]
86. Zhu, S.; Zhang, Y.; Zhu, B.; Zhang, J.; He, Y.; Xu, W. High cycle fatigue life prediction of titanium alloys based on a novel deep learning approach. *Int. J. Fatigue* **2024**, *182*, 108206. [CrossRef]
87. Han, S.; Khatir, S.; Wang, C.; Wahab, M.A. An improved Artificial Neural Network for the direct prediction of fretting fatigue crack initiation lifetime. *Tribol. Int.* **2023**, *183*, 108411. [CrossRef]
88. Tognan, A.; Patanè, A.; Laurenti, L.; Salvati, E. A Bayesian defect-based physics-guided neural network model for probabilistic fatigue endurance limit evaluation. *Comput. Methods Appl. Mech. Eng.* **2024**, *418*, 116521. [CrossRef]
89. Salvati, E.; Tognan, A.; Laurenti, L.; Pelegatti, M.; De Bona, F. A defect-based physics-informed machine learning framework for fatigue finite life prediction in additive manufacturing. *Mater. Des.* **2022**, *222*, 111089. [CrossRef]
90. Monaco, E.; Rautela, M.; Gopalakrishnan, S.; Ricci, F. Machine learning algorithms for delaminations detection on composites panels by wave propagation signals analysis: Review, experiences and results. *Prog. Aerosp. Sci.* **2024**, *146*, 100994. [CrossRef]
91. Moradi, M.; Gul, F.C.; Zarouchas, D. A Novel machine learning model to design historical-independent health indicators for composite structures. *Compos. Part B Eng.* **2024**, *275*, 111328. [CrossRef]
92. Zhang, X.; Xiong, Y.; Pan, Y.; Xu, D.; Kawsar, I.; Liu, B.; Hou, L. Deep-learning-based inverse structural design of a battery-pack system. *Reliab. Eng. Syst. Saf.* **2023**, *238*, 109464. [CrossRef]
93. Helwing, R.; Hülsbusch, D.; Walther, F. Deep learning method for analysis and segmentation of fatigue damage in X-ray computed tomography data for fiber-reinforced polymers. *Compos. Sci. Technol.* **2022**, *230*, 109781. [CrossRef]

94. Gholizadeh, S.; Leman, Z.; Baharudin, B. State-of-the-art ensemble learning and unsupervised learning in fatigue crack recognition of glass fiber reinforced polyester composite (GFRP) using acoustic emission. *Ultrasonics* **2023**, *132*, 106998. [CrossRef] [PubMed]
95. Zhang, X.; Pan, Y.; Xiong, Y.; Zhang, Y.; Tang, M.; Dai, W.; Liu, B.; Hou, L. Deep learning-based vibration stress and fatigue-life prediction of a battery-pack system. *Appl. Energy* **2024**, *357*, 122481. [CrossRef]
96. Xu, X.; Liu, C. Physics-guided deep learning for damage detection in CFRP composite structures. *Compos. Struct.* **2024**, *331*, 117889. [CrossRef]
97. Tao, C.; Zhang, C.; Ji, H.; Qiu, J. Fatigue damage characterization for composite laminates using deep learning and laser ultrasonic. *Compos. Part B Eng.* **2021**, *216*, 108816. [CrossRef]
98. Kolodziejczyk, F.; Mortazavi, B.; Rabczuk, T.; Zhuang, X. Machine learning assisted multiscale modeling of composite phase change materials for Li-ion batteries' thermal management. *Int. J. Heat Mass Transf.* **2021**, *172*, 121199. [CrossRef]
99. Srivastava, V.; Basu, B.; Prabhu, N. Application of Machine Learning (ML)-based multi-classifications to identify corrosion fatigue cracking phenomena in Naval steel weldments. *Mater. Today Commun.* **2024**, *39*, 108591. [CrossRef]
100. Sepasdar, R.; Karpatne, A.; Shakiba, M. A data-driven approach to full-field nonlinear stress distribution and failure pattern prediction in composites using deep learning. *Comput. Methods Appl. Mech. Eng.* **2022**, *397*, 115126. [CrossRef]
101. Cristiani, D.; Falcetelli, F.; Yue, N.; Sbarufatti, C.; Di Sante, R.; Zarouchas, D.; Giglio, M. Strain-based delamination prediction in fatigue loaded CFRP coupon specimens by deep learning and static loading data. *Compos. Part B Eng.* **2022**, *241*, 110020. [CrossRef]
102. Moradi, M.; Broer, A.; Chiachío, J.; Benedictus, R.; Loutas, T.H.; Zarouchas, D. Intelligent health indicator construction for prognostics of composite structures utilizing a semi-supervised deep neural network and SHM data. *Eng. Appl. Artif. Intell.* **2023**, *117*, 105502. [CrossRef]
103. Yan, C.; Vescovini, R.; Dozio, L. A framework based on physics-informed neural networks and extreme learning for the analysis of composite structures. *Comput. Struct.* **2022**, *265*, 106761. [CrossRef]
104. Zhang, Z.; Gu, G.X. Physics-informed deep learning for digital materials. *Theor. Appl. Mech. Lett.* **2021**, *11*, 100220. [CrossRef]
105. He, G.; Zhao, Y.; Yan, C. MFLP-PINN: A physics-informed neural network for multiaxial fatigue life prediction. *Eur. J. Mech.-A/Solids* **2023**, *98*, 104889. [CrossRef]
106. Jimenez-Martinez, M.; Alfaro-Ponce, M. Effects of synthetic data applied to artificial neural networks for fatigue life prediction in nodular cast iron. *J. Braz. Soc. Mech. Sci. Eng.* **2021**, *43*, 10. [CrossRef]

Disclaimer/Publisher's Note: The statements, opinions and data contained in all publications are solely those of the individual author(s) and contributor(s) and not of MDPI and/or the editor(s). MDPI and/or the editor(s) disclaim responsibility for any injury to people or property resulting from any ideas, methods, instructions or products referred to in the content.